The power of polymer wrapping

Salazar Rios, Jorge

Chapter 1

Introduction

1.1 The discovery of Single-Walled Carbon Nanotubes

In 1984, Sir Harold W. Kroto, at the invitation of Bob Curl, visited Rice University in Houston, Texas. That visit has had a lasting effect on nanoscience. In Houston, the two researchers met with Rick Smalley and the three scientists laid the foundation for future collaboration, one result of which was the Nobel Prize in chemistry, awarded to Kroto, Curl, and Smalley in 1996.

The joint project's initial objective was a further understanding of the formation in the space of long-chain carbon molecules using a laser-vaporization machine to simulate conditions in a red giant. In the course of the study, the researchers found, serendipitously, an extremely stable carbon allotrope composed of 60 carbon atoms. The structure of the new molecule resembled a soccer ball, so they called it buckminsterfullerene after R. Buckminster Fuller, the American architect known for geodesic domes.[1]

The discovery of C60 brought increased interest and attention to the research on carbon allotropes. In 1990, Wolfgang Krätschmer at the Max Planck Institute for Nuclear Physics in Heidelberg, Germany, and Donald Huffman of the University of Arizona in Tucson, USA reported the production of macroscopic quantities of C60. The buckminsterfullerenes were produced by putting two graphite electrodes into contact in a helium atmosphere and passing an electrical current between them.[2] In 1991, Sumio Iijima, a microscopist at the NEC Corporation Laboratories in Tsukuba, Japan, found another carbon allotrope called carbon nanotube. Inspired by the work from Krätschmer and Huffman, Iijima used a similar setup, but he placed the anode and the cathode at some distance; the difference created a spark between the graphite electrodes, and the reaction produced the growth of carbon needles on the cathode.[3]

Although Ijima's findings brought worldwide attention to carbon nanotubes for the first time, a similar reaction could have been produced in the late nineteenth century as a coincidence of chemical experimenting on methane.[4] In fact, in 1952, Radushkevich and Lukyanovich reported TEM evidence of some nano-sized tubular carbon filaments in the Journal of Physical Chemistry of Russia. However, the lack of access to Russian scientific publications during the cold war limited worldwide attention.[5]

The carbon nanotubes discovered by Iijima looked like concentric, atomically thick carbon sheets, ranging in number between 2 and 50 and rolled into tubes. These tubes formed by multiple graphene sheets were named multi-walled carbon nanotubes. Because of a large number of interactions among the graphene sheets, the theoretical predictions concerning the physical properties of the multiwalled carbon nanotubes have been cumbersome. However, the presence of carbon nanotubes formed by graphene sheets did allow theoreticians to predict single-walled carbon nanotubes (SWNTs). Furthermore, SWNTs

were predicted to be extremely rigid structures that would behave either as conductors or as semiconductors, as discussed below.[4]

Two years after Iijima found multi-walled carbon nanotubes, his team synthesized their single-walled counterparts.[6] Simultaneously, Donald Bethune's group at IBM's Almaden Research Center in San Jose, California achieved the same goal.[7] In June 1993, Nature published both works in a single issue, showing that the growth of SWNTs was promoted by mixing iron[6] or cobalt[7] into the graphite electrodes.

1.2 Describing Single-Walled Carbon Nanotubes

SWNTs are of keen interest both from a fundamental scientific point of view as well as for technological applications. SWNTs can be described as a single graphene sheet rolled up to form a tubular structure with a diameter between 0.4 and 3.0 nm.[8,9] The length to diameter ratio of the tubes can reach values above 100,000,000:1.[10,11] Due to such an impressive aspect ratio, the dangling bonds and cylinder end-caps at the extremes of the SWNTs can usually be ignored when describing the properties of the tubes.

A graphene sheet is a periodical arrangement of carbon atoms organized in a honeycomb structure. Each carbon atom is hybridized in an sp^2 configuration with three neighboring carbon atoms. The rolling up of the graphene sheet to form the carbon tube changes the system from 2D into 1D, inducing the quantum confinement of the electrons in two dimensions, which gives SWNT their unique properties.[12]

The quantum confined electrons can propagate only along the nanotube axis. For this reason, the wave vector $\vec{k}_{\parallel}$ is continuous, while the wave vector $\vec{k}_{\perp}$, when perpendicular to the axis, needs to satisfy a periodic boundary condition along the circumference. This implies that only quantized values are allowed for $\vec{k}_{\perp}$.[13] As a consequence, the density of states is marked by a set of sharp peaks called van Hove singularities.[14]

The density of states is fundamental to an understanding of the electronic structure of SWNTs, which can be defined by the cross-sections of the allowed $\vec{k}_{\perp}$ with the energy dispersion of graphene as shown in Figure 1.1. When $\vec{k}_{\perp}$ crosses the K points of graphene (Dirac points), the bonding π orbitals that form valence states and the anti-bonding π^* orbitals that form conduction states cross at the Fermi level. As a consequence, the energy gap between valence and conduction bands is closed, resulting in metallic SWNT. Otherwise, an energy gap is formed by the two parabolic bands, resulting in semiconducting SWNTs (s-SWNTs).[15] The bandgap (E_g) for the semiconducting species is inversely proportional to their diameter in agreement with confinement arguments and based on the tight-binding model approximation.[12]

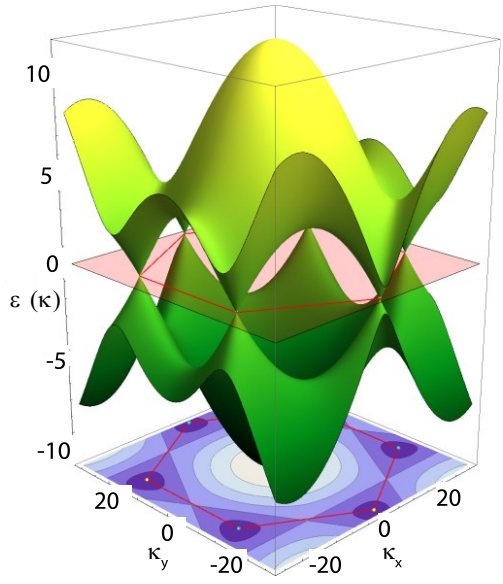

Figure 1.1. 2D energy dispersion relation of graphene in a nearest neighbour tight-binding model, the six Dirac points are depicted by the hexagon formed where the conduction and the valance band meet. Adapted from Ref.[16]

Every SWNT can be represented using the chiral vector $\vec{C}_h$ as shown in Figure 1.2, which is defined as

$$\vec{C}_h = n\,\vec{a}_1 + m\,\vec{a}_2 = (n,m) \tag{1.1}$$

Where $\vec{a}_1$ and $\vec{a}_2$ are the graphene lattice unit vector in real space and (n,m) are the translational indices of the hexagonal lattice. The SWNT is formed when the graphene sheet is rolled up to superimpose the two endpoints of the vector $\vec{C}_h$. Therefore, the magnitude of the chiral vector determines the diameter of the SWNT and the translational indices determine the direction in which the graphene sheet is rolled. Due to the hexagonal symmetry of the graphene lattice, the chiral angle Θ, between the vectors $\vec{C}_h$ and $\vec{a}_1$ can assume values between 0^o and 30^o, where the chiral indices need to fulfil the condition of $0 \leq m \leq n$.[17]

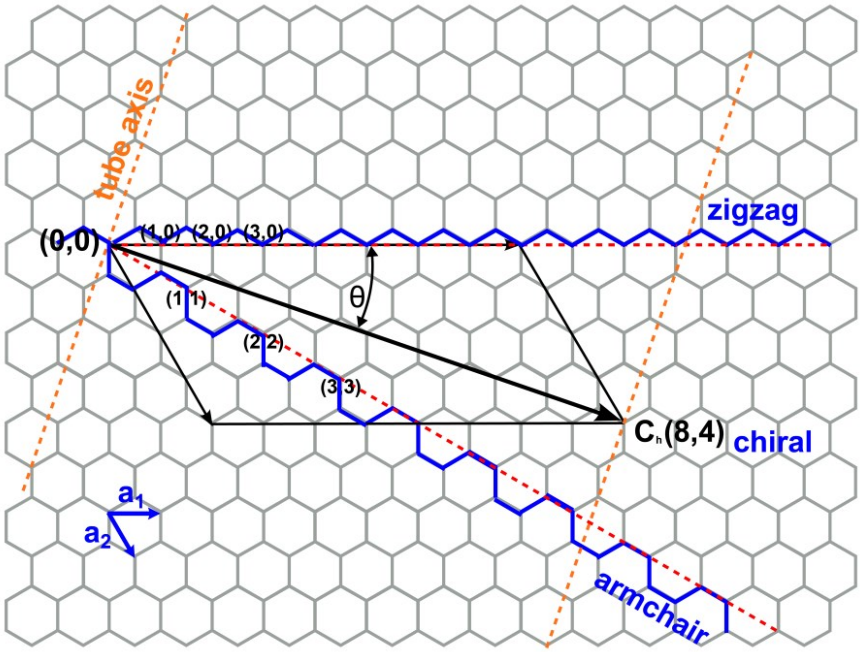

Figure 1.2. Honeycomb graphene lattice with the lattice vectors $\vec{a}_1$ and $\vec{a}_2$ and the chiral vector $\vec{C}_h$ that defines the unit cell of a (8,4) nanotube. The pattern along the circumference of zig-zag and armchair nanotubes are shown in blue. Adapted from Ref.[18]

The value of the chiral angle divides the different species of SWNT into three groups. At Θ=0°, it implies that m=0, and the SWNTs are called zig-zag tubes, because the carbon atoms form a zig-zag pattern along the circumference as can be seen in Figure 1.2. If Θ=30° then m and n are equal, and those tubes are called armchairs. The last and most abundant group is the so-called chiral SWNTs where $m \neq n \neq 0$.

Additionally, each of the SWNT species is either metallic or semiconducting, determined by the crossing of the π orbitals and the anti-bonding π^* orbitals at the Fermi level. Theoretically, in a sample of SWNTs, there are approximately one-third metallic SWNTs and two-third semiconducting SWNTs. In practice, the chiral indices (n,m) of each of the species give information about the electronic properties of the SWNTs. Figure 1.3 show the density of states (DOS) of a metallic armchair (6,6) and a semiconducting chiral (7,5) carbon nanotubes. When $|n-m| = 3q$ (where q is an integer), the nanotube is metallic. In any other case, the nanotubes are semiconducting.[19,20] The chirality and diameter distribution of the SWNT in a sample depends on the method used to synthesize them. There are several methods to produce SWNTs, each with different outcomes in resulting nanotube quality, quantity, purity and size distribution.

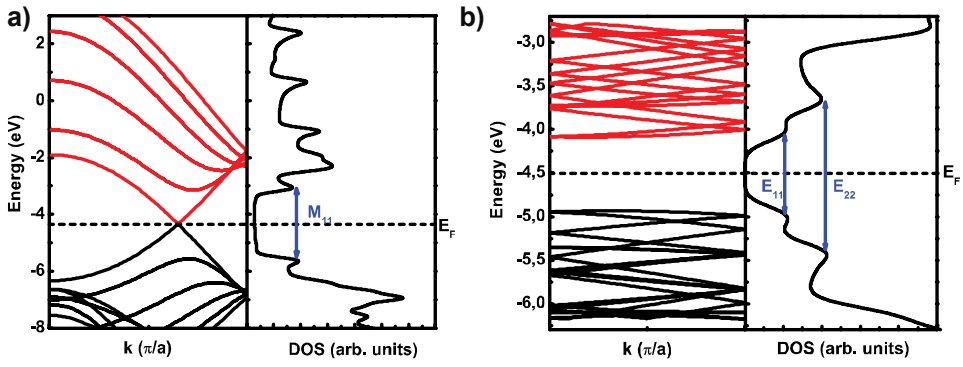

Figure 1.3. DOS obtained using density functional-based tight binding (DFTB) method for (a) metallic armchair (6,6) and (b) semiconducting chiral (7,5) carbon nanotubes (courtesy of Prof. Maria Cristina Dos Santos).[21]

1.3 Synthesis of Single-Walled Carbon Nanotubes

The first SWNTs were synthesized by arc-discharge (AD).[6,7] In the AD method, a direct current creates a high temperature between the carbon electrodes, which results in the vaporization of one of them. This method produced tubes with few structural defects, but the yield is generally low.[22] After improvements in operational parameters and catalyst composition, the output quantities of AD increased significantly.[23,24] In order to increase the yield for semiconducting nanotubes, the graphite anode is usually mixed with transition metals such as Fe, Co, Ni, Y. The resulting nanotubes, so-called SO nanotubes, have a typical diameter of around 1.5 nm and typically lie in a length range between 1 and 5 μm.

Another method to produce SWNTs is through chemical vapor deposition (CVD), used for the first time by José−Yacamán *et al.*[25] Currently, large scale CVD is the most popular method due to the high proportion of semiconducting over metallic SWNTs species with roughly 2/3 ratio of semiconducting SWNTs.[26,27] CVD usually involves the flow of a gaseous hydrocarbon source over metal catalyst particles such as Fe, Co or Ni under the influence of either heat (thermal CVD) or plasma irradiation (plasma-enhanced CVD).[28–30] Catalytic CVD (CCVD) is on the market with different catalyst producing SWNTs of different diameters on a large scale. The best-known SWNTs produced by CCVD are the so-called HiPCO (high-pressure CO) tubes with diameters between 0.8 and 1.2 nm, and CoMoCAT (Co and Mo catalyst) tubes with diameters between 0.7 and 0.9 nm.

In recent years, Plasma torched discharge (PD) and Tuball SWNTs appeared on the market. The PD process reaches outputs in the range of kg/day of high-quality SWNTs with diameters in the range of 1.2-1.6 nm.[31] PD SWNTs have a lower defect density and considerably longer individual tubes lengths compared to other SWNTs sources.[23,32,33]

The Tuball process produces SWNTs with diameters of 1.4-2.2 nm, and are the lowest costing on the market.[34]

The various commercial techniques can produce large quantities of SWNTs with a low density of structural defects. However, it is not yet possible to control the chirality and thereby the electronic characteristics of the tubes merely through synthesis. For the application of SWNTs in electronics, a high concentration of s-SWNTs in the final sample is required. Small-scale CVD systems can achieve samples containing more than 95% semiconducting species.[35–37] For real-world electronic applications, however, semiconducting SWNT of purity > 99.99% are necessary.[38,39] As a consequence, post-growth treatments are required to separate semiconducting from metallic SWNTs.

1.4 Selection of semiconducting Single-Walled Carbon Nanotubes

Post-growth treatments for SWNTs are divided into two main groups, the central difference between them being the type of functionalization of the SWNTs. In one case, the walls of the tube are functionalized covalently, while non-covalent functionalization is used in the other.[40] SWNTs have been functionalized covalently since 1998, with the goal of increasing their solubility by modifying the side walls or the open ends of the tubes.[41,42] Covalent functionalization has also been demonstrated to enable the discrimination of SWNTs based on their electronic structure.[42,43] However, because the non-reversible covalent functionalization by disrupting the tube walls affects the physical and electronic properties of the tubes,[44] the main advantage of non-covalent functionalization is that the initial properties of the SWNT are only minutely affected after the functionalization.[45]

One of the most successful non-covalent functionalization strategies uses surfactants such as Sodium dodecyl sulphate (SDS),[46] sodium dodecylbenzene sulphonate (SDBS),[47] or sodium cholate (SC) in water.[48] These molecules have a hydrophobic group (tail), which interacts with the nanotube wall, and a hydrophilic group (head), which interacts with water. While this technique allows for isolating the individual tubes and solubilizing them, the surfactants do not differentiate between metallic and semiconducting tubes, and these species can therefore not be separated. The individualization of SWNTs, however, has been instrumental in understanding the physical properties of single tubes,[49] since SWNTs have the natural tendency to bundle in relatively large assemblies because of the van der Waals forces. Nonetheless, different procedures had to be devised in order to isolate semiconducting SWNTs.

The first method used to sort SWNT of different electronic nature was by density gradient ultracentrifugation(DGU),[48] which uses the different densities of SWNTs that have been pre-treated with surfactants. In this method, the SWNT sample is first mixed with a surfactant and loaded into a medium with a known density gradient. In general, large

diameter nanotubes have a lower density than small diameter species. Separation based on electronic properties has also been achieved by using a mixture of sodium dodecyl sulfate (SDS) and sodium cholate (SC), as the two surfactants interact differently with tubes of different polarizability.[48] The result is a multi-layer colored solution, where the different colors indicate tubes of slightly different band gaps. This technique can generate samples which contain around 99% s-SWNTs.[50] The position of the different layers in the medium is controlled by changing the ratio of the surfactants.[51]

Another technique invented in the last decade to purify s-SWNTs is gel chromatography. As the name indicates, it is a chromatographic technique, where a gel is used as a medium, and several columns are connected vertically in series. The SWNTs are first dispersed with a surfactant and are embedded on top of the first column with an allyl dextran/based gel. The surfactant coverage varies depending on the curvature of the SWNT. As a consequence, the nanotubes are absorbed in different columns depending on the interaction strength of each tube with the gel. This strength is related to the magnitude of the van der Waals force between the SWNTs and the gel in the chromatography column. Nanotubes with a different curvature will have a different surfactant coverage. Thus, they will exhibit different interaction strengths with the gel. During the sorting process, only the nanotubes with the highest interaction strength remain in the column.[52] After one chromatographic cycle, the purity of the s-SWNT in the sample can be up to 95%.[53]

Having been dispersed by a surfactant, SWNTs can also be sorted through the application of an alternating electric field. This technique is called dielectrophoresis and is based on the difference in polarizability between metallic and semiconducting tubes. The higher polarizability of the metallic SWNT leads to a migration (in the liquid) of the tubes towards the electrodes, while semiconducting tubes remain in a stationary position.[54] The main drawback of this method is the limited throughput.

In this thesis, one additional method was selected to sort s-SWNTs, the so-called π-conjugated polymer wrapping technique. This technique is used due to its simplicity, effectiveness and scalability.

1.5 Polymer-Wrapped Single-Walled Carbon Nanotubes

In 1999, the group of Adam Strevens reported the first attempt to disperse SWNTs using polymers, where the polymer poly(m-phenylenevinylene-co-2,5-dioctoxy-p-phenylenevinylene) (PmPV) was used to disperse SWNT.[55] However, the first demonstration that a conjugated polymer could separate s-SWNTs from metallic SWNTs (m-SWNTs) came in 2007, when Nish *et al.* functionalized SWNT using a polyfluorene-based polymer dissolved in an organic solvent.[56]

The first step of the polymer wrapping technique is to dissolve the π-conjugated polymer in an organic solvent. The polymer is then mixed with the SWNT sample. Due to the relatively strong van der Waals interaction between their walls, SWNTs initially form in bundles. Ultrasonication is applied to individualize the tubes, which allows for the conjugated polymer chain to interact with the individualized SWNTs. The strength of the SWNT:polymer interaction must be stronger than the interaction of each component with the solvent (toluene) in order to create a stable hybrid composed of the polymer chain wrapped around the SWNT wall.

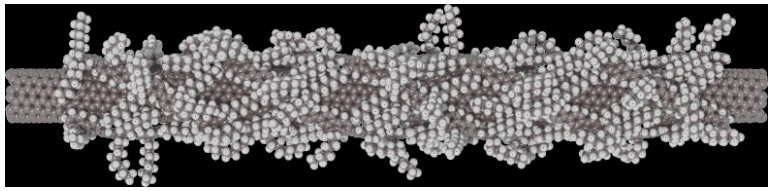

Figure 1.4. Simulation of polymer backbones forming helical structures around a SWNT.

The SWNT:polymer interaction is a complex process that is still a subject of investigation. Earlier, it was proposed that the interaction was dominated by the interaction between the π-electrons in the two systems, and that the polymer backbone was primarily responsible for the interaction.[56] The conjugated polymer acquires a helical conformation around the tube as has been shown by Gao *et al.,* and depicted in figure 1.4.[57] Gomulya *et al.,*[58] have demonstrated that the alkyl chains also play a significant role in the selection process determining the diameter of the selected tubes and stabilizing the complex.

It has been proposed that the coverage of the SWNT wall by the conjugated polymer partially screens the polarizability of the SWNTs, and that this screening is proportional to the coverage.[59] Due to the higher polarizability of the metallic species compared to the semiconducting SWNTs, partially covered s-SWNT can be individualized, but m-SWNTs with similar polymer coverage re-aggregate in bundles.[60,61] To date, different π-conjugated polymers have been used for the dispersion and selection of s-SWNT. Each of these polymers offers different dispersion yields and chirality selectivity depending on the backbone structure and the length of the lateral alkyl chains.[62–67]

After the individualization of the s-SWNT species, the polymer:SWNT ink remains a mixture with metallic bundles and free polymer chains. For this reason, a centrifugation step is required. When the ink is centrifuged the heavy bundles precipitate, and the individualized s-SWNT remain in the supernatant together with the free polymer chains. At this point the supernatant can be extracted; this phase produces high purity individualized s-SWNTs at relatively low concentration and a large amount of excess polymer.[57,68]

An important contribution to the possibility of utilizing the SWNTs inks arose with the discovery that a second centrifugation step performed at a higher speed and for a longer time could force the wrapped s-SWNT to precipitate while keeping the free polymer chains in the supernatant.[69] The precipitated and highly pure s-SWNTs can then be re-dispersed in a solvent, allowing adjustments of concentration and making the inks ready for different applications. The step-by-step phases of the sorting process discussed above is represented in Figure 1.5. After the inks are prepared, characterization is crucial before they can be used for the fabrication of electronic devices.

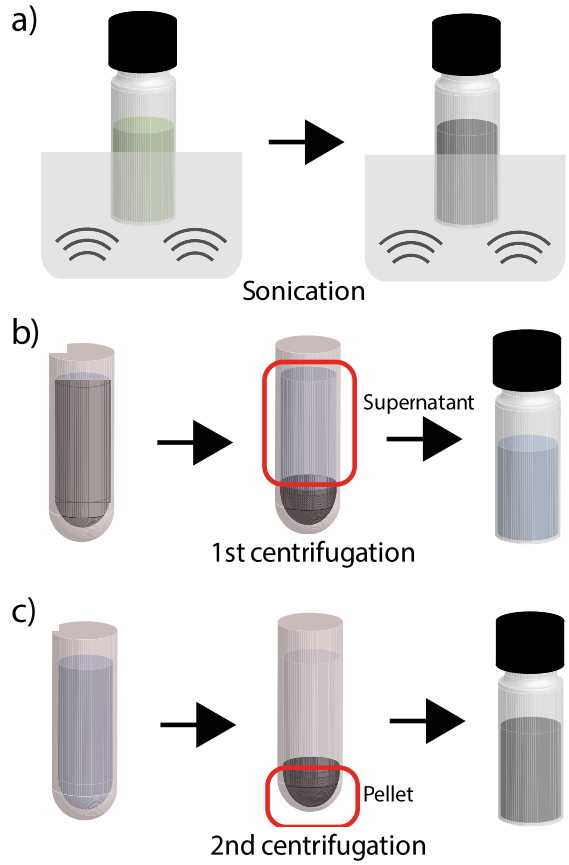

Figure 1.5. a) Ultrasonication of the mixture of conjugated polymer and SWNT. b) First centrifugation to extract the supernatant composed by individualized s-SWNTs and polymer chains. c) Second centrifugation to extract and re-disperse the pellet of s-SWNTs wrapped with polymer chains (excess polymer is removed in the supernatant).

1.6 Characterization of semiconducting Single-Walled Carbon Nanotube inks

Due to the quantum confinement of the SWNTs and the differences in the electronic properties of metallic and semiconducting species, optical characterization is an effective method to study s-SWNT samples. UV-vis absorption provides information about the species of s-SWNTs present in the sample. As a consequence of the van Hove singularities, each nanotube species exhibits an absorption peak at a specific wavelength, giving rise to a very precise fingerprint of their nature. The absorption transition will depend on the diameter and on the chirality of the tubes. Shifts in the absorption can also be detected depending on the environment, namely the nature of the solvent and the wrapping polymer.[70] For semiconducting tubes between 0.8-1.2 nm diameter, the first electronic transitions, E_{11}, lie between 1000 nm and 1600 nm, and the second, E_{22}, are between 600 nm and 900 nm. For metallic species, the first transitions M_{11} are between 500 nm and 600 nm, which is indicated in Figure 1.6.

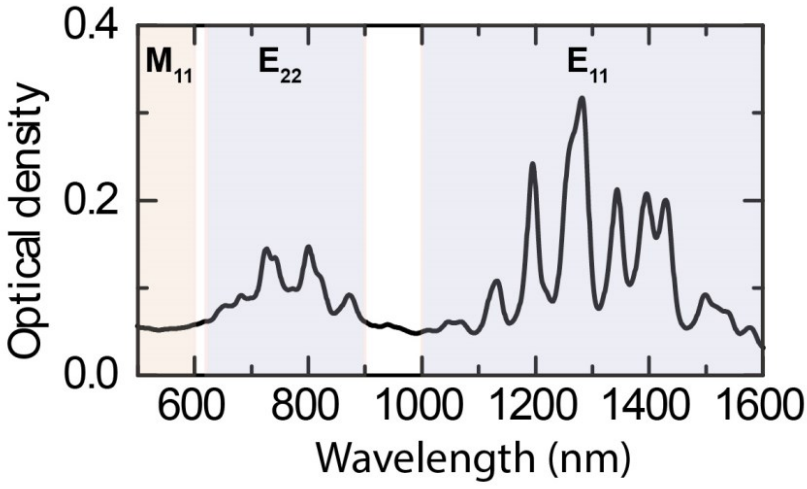

Figure 1.6. Absorption spectra of a sample of SWNTs wrapped by a polyfluorene derivative.

When the tubes are bundled, the interactions among them broaden their electronic transition, and it is difficult to differentiate between the different species. In contrast, when the tubes are individualized, each sharp peak in the absorption spectrum represents a distinct SWNT chirality. The absorption measurements also furnish information about the interaction between the polymer and the tubes. In the specific case of polythiophene derivatives, when the polymer is planarized as a consequence of the interaction with the SWNT, two peaks appear around 500 nm appears, which can be seen in Figure 1.7.[71]

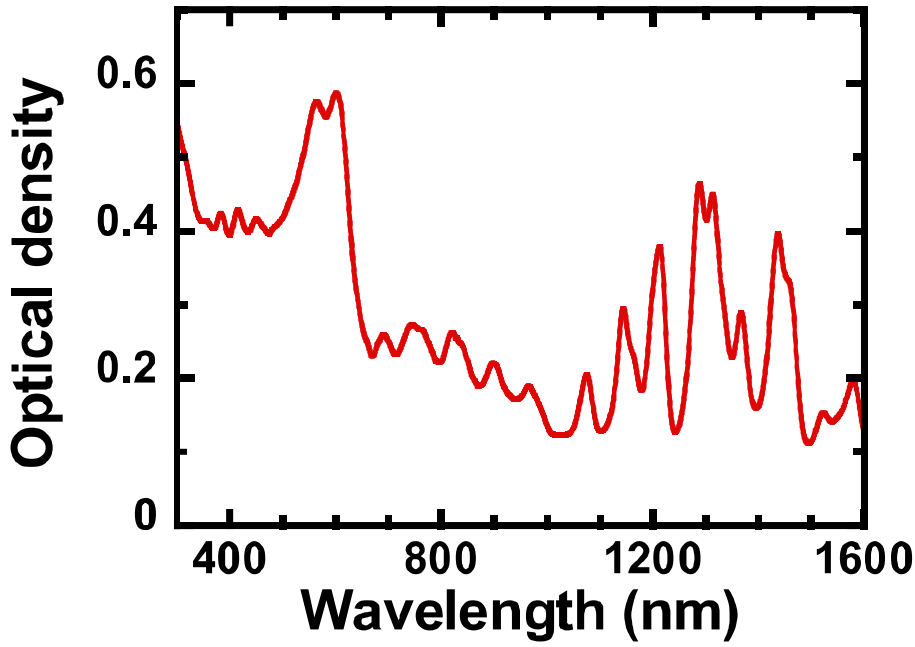

Figure 1.7. Absorption spectra of s-SWNT selected by a polythiophene derivative. The two peaks around 500 nm indicate the crystallization of the polymer.

Another optical technique that will be used in this thesis is photoluminescence (PL) spectroscopy. The photoluminescence intensity is extremely sensitive to the nature of the SWNTs, their bundling and the interaction with the wrapping polymer and the solvent. Time-resolved PL provides information about the decay pathways in the sample. When s-SWNTs are not individualized the number of possible decays increases, and the PL lifetime becomes shorter.[72]

The high stability and excellent charge carrier transport of SWNTs make them appealing for application in electronic devices, such as field effect transistors and solar cells. One of the ultimate tests for the purity of the solutions is the fabrication of field effect transistors. This technique will be amply used in the thesis.

1.7 Fabrication of field effect transistors using Single-Walled Carbon Nanotubes

The excellent charge transport properties along the axis of s-SWNTs is one of the main reasons that has stimulated scientists to find methods to sort semiconducting SWNTs. One important application foreseen for s-SWNTs is their use in field effect transistors (FETs). Twenty-six years after their discovery, SWNTs, owing to their dimensionality, are still

considered to be the material that can allow further miniaturization after the end of Moore's law for Si.[73–75] Tans *et al.* demonstrated for the first time a single SWNT device in which ballistic transport was achieved.[76] However, single nanotube devices are not easily mass-produced; in fact, the first examples were only statistically produced. Recently, however, with the advent of the new solution-based sorting techniques, effective self-assembly methods have been demonstrated.[64,77] In addition to single nanotubes devices, networks of SWNT FETs are also appealing, as they can be mass produced easily with solution-based techniques, and their fabrication has been proven possible with ink jet printing, blade coating and slot-dye coating.[78–81] Snow *et al.* reported the first example of the SWNTs network FETs. These transistors were fabricated by growing a network of SWNTs on top of the thermal oxide of a conducting Si substrate.[82] In this thesis, network FETs will be reported not only as a method to characterize the quality of the SWNT inks but also because of the heightened interest in their application.

1.7.1 Single-Walled Carbon Nanotubes field effect transistor operation and characterization

A FET is a three terminal device composed of a source, a drain and a gate electrode. Charges travel from the metal source to the drain through a semiconducting active channel that is on top of a gate insulating layer. The structure of a FET is shown in figure 1.8. The active channel is defined by the distance between the source and the drain electrode (L) and by the width of those electrodes (W). The charge transport in the FET is modulated by the gate bias, which controls the accumulation or depletion of charge carriers at the insulator/semiconductor interface in the channel.[83] This modulation is the basis for the fabrication of logic devices and is the foundation of computing technology.

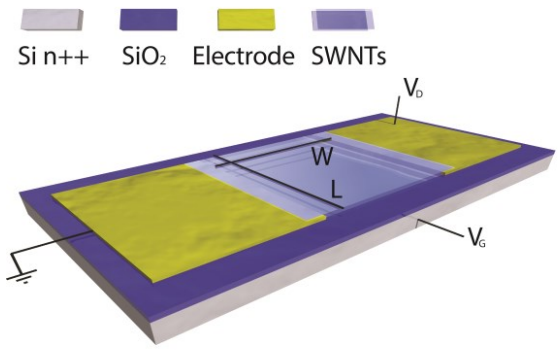

Figure 1.8. Schematic structure of a SWNT FET with SiO_2 as a dielectric layer and a heavily doped Si as the gate contact. W is the width of the source and the drain, L is the distance between source and drain, V_D is the drain voltage and V_G is the gate voltage.

FETs fabricated using s-SWNTs are intrinsically ambipolar, meaning that they can operate in hole and electron accumulation mode, depending on the applied gate bias. If the gate voltage is negative ($V_G < 0$), the interface between the dielectric and the active channel will accumulate positive charges as shown in Figure 1.9a.

When a voltage V_D is applied, the positive charges in the active channel will flow from drain to source, creating a current I_{DS}, which is depicted in figure 1.9b. This process is called p-channel operation of a FET. In the case of an n-channel operation of a FET the opposite occurs. When a $V_G > 0$ is applied, there will be an accumulation of positive charges at the gate, and negative charges will be induced at the interface.

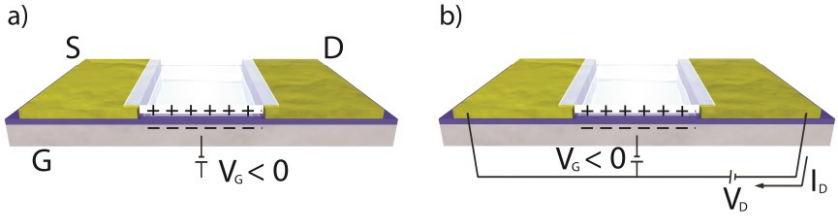

Figure 1.9. Scheme of the operation of p-type FET. a) Charge accumulation in the active channel induced by a negative gate voltage. b) I_{DS} current generated as consequence of the applied V_D.

While there are many examples of ambipolar devices fabricated with polymer wrapped SWNTs in the literature,[69,84,85] in practice, SWNT FETs often operate in a unipolar mode with a hole dominated transport. This is due to the modification of the SWNT DOS by the wrapped polymer, [71,79] the exposure to oxygen[86] and the location of the SWNTs valence

band with respect to the metal contacts used for the electrodes that facilitate the injection and transport of holes.[87]

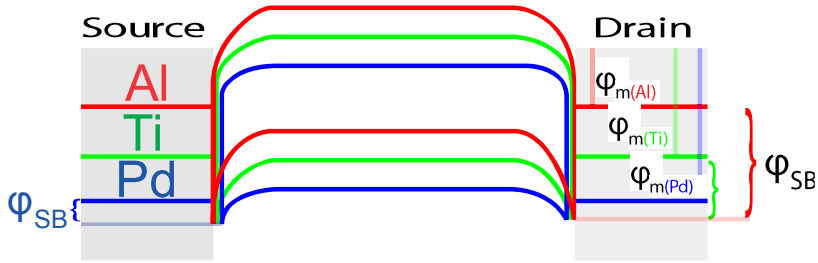

Figure 1.10. Band alignment of (8,7)s-SWNT with different metals. The different work functions determine the Schottky barrier (φ_{SB}). Adapted from Ref.[87]

As illustrated in Figure 1.10, Pd shows a smaller injection barrier for holes (φ_{SB}) compared to the Al and Ti, due to the location of the valence band (VB) of SWNTs with respect to the work function (φ_m) of the metals. However, there is still a remaining injection barrier between the metal contact and the active layer due to energy barrier pinning, and the pinning of the energy barrier determines the final value of the injection barrier. Formation of the injection barrier is a complex process that encompasses the interplay of φ_m, the ionization potential of the SWNTs and also the interfacial-dipole induced at the interface by different chemical species.[88] While the height of the barrier is approximately determined by the nature of the tube and of the metal, the width can be tuned by the applied drain or gate bias.[89]

The injection barrier width for hole transport is reduced when the negative gate bias is applied. As a consequence, charges can be transported through the barrier via thermal excitation or via tunneling. Both processes are involved in the charge transport, and they are commonly referred to as thermionic emission. The proportion of these processes is highly dependent on the given applied bias and the operating temperature. One way to determine the injection barrier is by the contact resistance (R_c) that is governed by a power law dependency with the gate bias and the temperature.[90]

R_c influences the FET operation as a series resistance in the drain-source circuit. This series resistance is the sum of the channel resistance R_{ch} and the contact resistance R_c and is described as,

$$R_{tot} = \frac{V_{DS}}{I_{DS}} = R_{Ch}(L) + R_C = \frac{L}{WC_i\mu(V_{GS} - V_{TH})} + R_D + R_S \tag{1.2}$$

where C_i is the capacitance of the dielectric layer per area (F/cm^2), μ is the mobility of the active layer (cm^2/Vs) and V_{TH} is the threshold voltage that represents the potential bias onset for the inversion regime. For conventional Si-FETs, the threshold voltage is defined as the gate bias where the Fermi level at the insulator-semiconductor interface crosses the

middle of the bandgap. However, in SWNT FETs the determination of the V_{TH} is not straightforward and is highly dependent on the shallow traps that are filled prior to the inversion regime transition, as is found in the case of organic FET.[91]

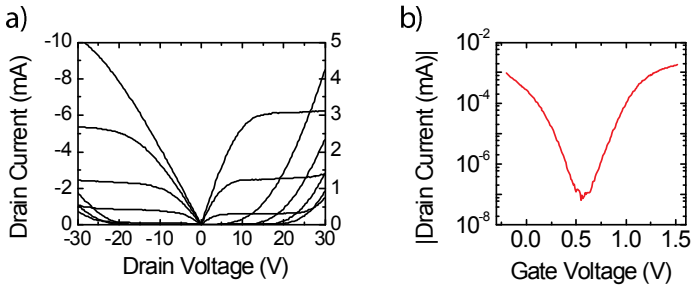

Figure 1.11. SWNT FET electrical characteristics. (a) I-V characteristics (or output characteristic) and (b) transfer characteristics.

There are two types of measurements needed for the quantification of the figures of merit of FETs. These are the I-V characteristics (an example is shown in 1.11a) and the transfer characteristic (an example is reported in Figure 1.11b).

The transfer characteristics are measured by sweeping the gate potential and probing the drain-source current (I_{DS}) while keeping the drain potential constant throughout the sweeping. This curve can be used to extract the linear mobility μ_{lin}, the saturation mobility μ_{sat}, the V_{TH}, the on/off ratio and the sub-threshold swing in the so-called direct method (DM).

The V_{TH} can be determined using the zero interception of the transconductance g_m slope.[92] The on/off ratio is defined by the ratio of the highest and the lowest drain-source current measured, and this represents the on and off state of a logic gate (i.e., the transistor). The sub-threshold swing is defined as the change in gate voltage which must be applied to increase the output current by one decade, and it provides information about the interface and bulk trap densities of the FET.[93]

For calculating the linear and the saturation mobility, the following relations are obtained by the gradual channel approximation model,

$$\mu_{lin} = \frac{L}{WC_iV_{DS}}\left[\frac{dI_{DS}}{dV_G}|_{V_{DS}}\right] \tag{1.3}$$

$$\mu_{sat} = \frac{2L}{WC_i}\left[\frac{dI^{1/2}{}_{DS,sat}}{dV_G{}'}\right]^2 \tag{1.4}$$

where V_G' is V_G-V_{TH}. For the calculation of the saturation mobility (μ_{sat}), the mean value of charges in the conduction channel is used to define the charge density. In practice, however, the charge carrier density is not constant, with a maximum at the source contact and a minimum at the drain contact.[94] In the linear mobility (μ_{lin}) regime, the density of charge carriers is more homogenous compared to the saturation regime.[83] However, μ_{lin} also has several limitations and the value obtained has a large error when μ is gate-dependent or the injection barrier is high.

The second measurement method is the I-V characteristic or output characteristics (Figure 1.11a). The I-V curves are obtained by sweeping the drain potential while measuring I_{DS} and keeping the gate potential constant. The mobility can also be extracted from the output characteristic using the transfer length method (TLM). The extraction of the mobility using TLM is more complex than using the DM because several device lengths are required to obtain the desired parameters. The main advantage of the TLM is that it also allows extraction of the contact resistance, which is not possible with the direct method. Because the contact resistance is used for the calculation of the mobility value, the accuracy of the TLM method value is higher than the DM method.

The TLM method is performed by taking the slope of the linear regime of the output curve.[90] The slope (m) is derived from the R_{tot} (equation 1.2) using the relation given by

$$m = \frac{dR_{tot}W}{dL} = \frac{L}{\mu C_i V_G{}'} \tag{1.5}$$

where the slope of $R_{tot}W$ against the channel length gives the value of m. The mobility and V_{TH} can be extracted from plotting the reciprocal of m against the gate voltage, where

$$\mu = \frac{1}{C_i}\frac{dm^{-1}}{dV_G} \tag{1.6}$$

and the V_{TH} is the zero intersection of the corresponding slope.

An additional challenge when characterizing SWNT FETs is that the electrostatic coupling with the gate bias does not follow the standard parallel plate model. The parallel plate model is not suitable due to the limited coverage of the dielectric by the SWNT network, as explained by Cao *et al.*[95] Therefore it is necessary to use an effective capacitance which has the following expression:

$$C_{eff} = \Lambda_0^{-1}\left(\frac{1}{2\pi\varepsilon}\ln\left(\frac{\Lambda_0}{R\pi}\sinh\left(\frac{2\pi d}{\Lambda_0}\right)\right) + C_Q^{-1}\right)^{-1} \tag{1.7}$$

where Λ_0^{-1} is the linear density of the SWNT network in cm^{-1}, R is the SWNT average radius, C_Q is the SWNT quantum capacitance which has a value of $4x10^{-10}$ F/m, and d and ε are the dielectric thickness and the permittivity, respectively. The use of this relation allows for a more accurate mobility extraction. Earlier, the mobility for SWNT FETs devices with high capacitance had often been underestimated.

Figure 1.12 summarizes the state of the art of field effect transistors fabricated with different methods in previous years. SWNT FET fabrication is both instrumental for the optimization of the polymer-wrapped SWNTs inks and for the understanding of their quality and their possible application in technology.

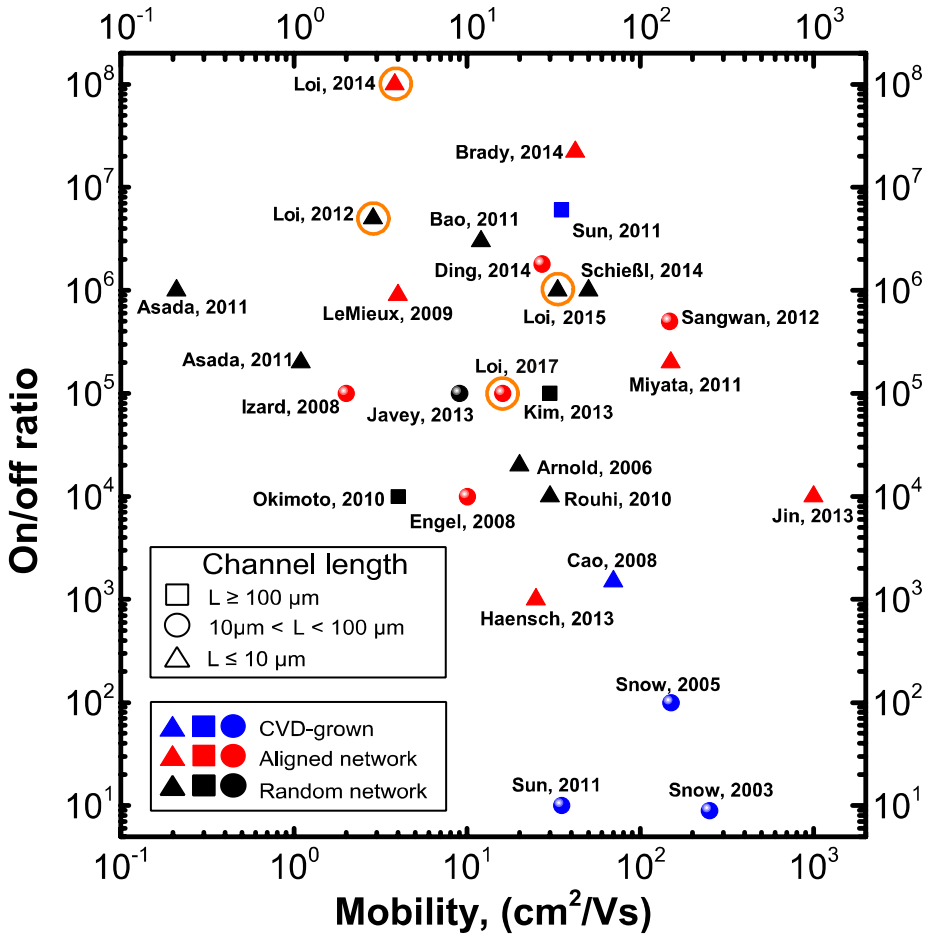

Figure 1.12. Performance map of SWNT FETs fabricated by CVD and solution-based processes. The orange circles indicated the works performed in the Loi group.[48,63,68,69,79,82,96,97]

1.8 Single-Walled Carbon Nanotubes in solar cells

Solar cells (SCs) are optoelectronic devices that are able to convert the light absorbed in a semiconductor. A solar cell comprises an active layer formed by one or more materials sandwiched between two metal electrodes. Commonly, electron and hole selective contact layers are inserted between the active layer and each electrode in order to increase the device performance.

Under illumination, depending on the nature of the semiconductor, electrostatically bound electron-hole pairs (excitons) or free carriers are formed by absorption of a photon. Special interfaces are employed to split the exciton and/or to avoid free carrier recombination. Finally, electrons and holes are extracted by two electrodes with adequate work functions.

In order to avoid recombination, heterostructures are fabricated, where the energy levels of the two materials are arranged in a type-two configuration. A p-n junction, because of the alignment of the Fermi level in the two materials, is a type II heterostructure.[83] Sometimes the metal can also be used to further separate the charges. These types of devices are called Schottky-junction solar cells.[98]

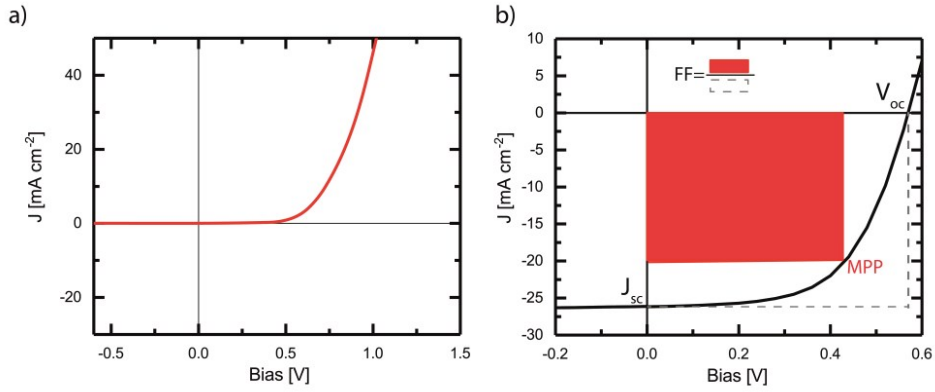

Figure 1.13. J-V curve of a solar cell. a) In the dark. b) Under illumination including the figures of merit of a solar cell.

The SC presents a diode-like behavior with a small current in reverse bias in the dark (Figure 1.13. a) governed by the shunt resistance, and an exponential increasing current in forward bias limited by the series resistance.

Under illumination, the current produced by the photogenerated charges flows against the applied bias, and power can be extracted from the device. The parameters to calculate the power conversion efficiency of the SC are illustrated in Figure 1.13b. At zero bias (V=0) no load is applied on the circuit, and the extracted current is defined as the short circuit current (J_{sc}). When the circuit is broken no current is extracted, and the built up charge carriers form the open circuit voltage (V_{oc}). This is the maximum voltage the SC can deliver. However, in both cases the power generated by the SC is zero (P= J·V).

In order to find the power conversion efficiency (PCE), the maximum power that can be generated (J_{MPP}, V_{MPP}) for the SC is divided by the power density (P_{in}) of the solar illumination incident on the surface of the device

$$PCE = \frac{J_{MPP} \cdot V_{MPP}}{P_{in}} \tag{1.8}$$

The other option is to use the fill factor (FF) that is defined by the ratio of the maximum area that can fit under the J-V curve in the fourth quadrant and the area defined by the product of the V_{oc} and the J_{sc}.

$$FF = \frac{J_{MPP} \cdot V_{MPP}}{J_{SC} \cdot V_{OC}} \tag{1.9}$$

In this case, PCE is defined as

$$PCE = \frac{J_{SC} \cdot V_{OC} \cdot FF}{P_{in}} \tag{1.10}$$

The outstanding semiconducting properties of SWNTs, including their stability and remarkable carrier mobility along the tube axis, have stimulated their application in solar cells.[99–101] However, several challenges have been encountered. First, their relatively small bandgap creates problems in finding another material with which to fabricate a type-II heterojunction. Second, their one-dimensional nature allows rather narrow absorption features, leading to a poor coverage of the solar spectrum. Third, the extreme aspect ratio of carbon nanotubes and their conduction along the tube axis makes the fabrication of diode structures challenging. The efficient transport in plane of s-SWNTs is beneficial for FETs with their planar geometry, but for SCs the transport needs to be out of plane because of the device geometry. When the SWNTs are lying on a substrate, the transport out of plane is cumbersome because the charge carriers are forced to hop from one SWNT multiple times in order to traverse the absorption layer.

As a consequence of all these challenges, attempts at using SWNTs as an active layer has achieved only modest results.[99–102] All-carbon based devices reported efficiencies under 1%,[99] Ultrathin carbon nanotube absorber films reached PCE of 1%,[100] and the innovative approach of s-SWNTs aerogel bulk heterojunction reached 1.7%.[101] However, SWNTs have been reported to be useful in the stabilization of different types of solar cells.

Commercially available devices are encapsulated by or coated with barriers to protect the active layer and electrodes from the environment. It has been demonstrated recently that the inclusion of an extra layer of s-SWNTs between the active layer and the electrodes is a possible strategy to maintain SC performance over longer time periods.[103] For instance, SWNTs have already been successfully incorporated in perovskite SCs to fulfill the double function of hole transporting layer and protecting layer to improve the stability of the devices.[103–106] This has been explained with the hydrophobicity of these nanocarbon materials, which results in the protection of the active layer from atmospheric humidity.[103]

1.9 Thesis outline

The understanding of the physico-chemical processes involved in the nanotube-polymer interaction can lead to the development of high-quality s-SWNT inks for the fabrication of high-performing electronic devices, such as FETs and SCs. This thesis not only reports investigations that aim to better understand the interaction mechanism between the conjugated polymer chains and the semiconducting SWNTs, but also reports applications of these high-quality inks in field effect transistors and solar cells.

In **Chapter 2**, the investigation of the interaction of three different conjugated polymers with SWNTs of two different diameters is described. poly[(4,4-di-n-dodecyl-4H-cyclopenta[2,1-b:3,4-b']dithiophene-2,6-diyl)-alt-(2,1,3-benzothiadiazole-4,7-diyl)] P12CPDTBT), poly(9,9-di-n-dodecylfluorene-2,7-diyl) (PF12) and poly(3-dodecylthiophene-2,5-diyl) (P3DDT) were mixed with SWNTs of different diameters. The results show that for small diameter SWNTs, the flexibility of the polymer backbone is crucial to increase the SWNT dispersion yield by means of an improved nanotube-polymer interaction. For SWNTs with a large diameter, the backbone flexibility is less important, and a bulkier chemical structure of the polymer backbone maximizes the surface coverage, thereby increasing the amount of individualized nanotubes in the final sample.

Chapter 3 demonstrates how the energy level alignment of two n-type conjugated polymers with the s-SWNTs affects the charge transport in FETs. The two polymers used to select s-SWNTs were poly{[N,N9-bis(2-octyldodecyl)-naphthalene-1,4,5,8-bis(dicarboximide)-2,6-diyl]-alt-5,59-(2,29-bithiophene)} (N2200) and poly{[(N,N′-bis(2-octyldodecyl)-1,4,5,8-naphthalenedicarboximide-2,6-diyl)-alt-5,5′-(2,2′-bithiophene)]-co-[(N,N′-bis(2octyldodecyl)-1,4,5,8-naphthalenedicarboximide-2,6-diyl)-alt-5,5′-(2,2′-(4,4'-dimethoxy bithiophene))]} (PE-N-73). The two narrow bandgap polymers have a different energy level alignment with the s-SWNTs. We found that when the valence band of the polymer and the s-SWNT have a similar position, the presence of the conjugated polymer does not affect the charge transport negatively. We also found that when the band alignment between the conjugated polymer and the s-SWNT is not ideal, the presence of extra polymer is harmful for the FET performance.

Chapter 4 describes how to control the polarity of s-SWNTs FETs by adding dopants directly to the s-SWNT ink. Benzyl viologen (BV), 4-(2,3-Dihydro-1,3-dimethyl-1H-benzimidazol-2-yl)-N,N-dimethylbenzenamine (N-DMBI) and 2,3,5,6-Tetrafluoro-7,7,8,8-tetracyanoquinodimethane (F_4-TCNQ) are used for this purpose. The field effect transistors fabricated with these doped inks show that BV and N-DMBI can enhance the electron transport properties of the s-SWNT ink, while F_4-TCNQ can largely transform the transistors into p-type. The investigation of different device structures allows for distinguishing between doping of the active layer via interaction of the dopant with the polymer wrapped SWNT from the interaction of the dopant with the electrodes.

Chapter 5 reports the use of s-SWNT as an interlayer for PbS colloidal quantum dot (CQD) SC. PbS CQD SCs are stable when stored in dark under ambient conditions. However, all the figures of merit reduce drastically after exposure to air under illumination. The addition of a s-SWNT interlayer between the active layer and the anode improves the stability of the devices dramatically without harming the figure of merit of the device. The photoconversion efficiency, the open circuit voltage, the short-circuit current and the fill factor remains almost constant for more than 100 h under AM1.5 illumination in ambient conditions.

Finally, **Chapter 6** contains a discussion on the feasibility of applying s-SWNT inks in the fabrication of flexible electronic devices with a perspective towards commercialization. Market opportunities for SWNT devices, challenges in the process of s-SWNT selection and the strengths of using SWNT inks for the fabrication of solution processable devices are discussed, focusing on the implementation of SWNTs in the current electronic device market.

1.10 References

[1] H. W. Kroto, J. R. Heath, S. C. O'Brien, R. F. Curl, R. E. Smalley, *Nature* **1985**, *318*, 162.

[2] W. Krätschmer, L. D. Lamb, K. Fostiropoulos, D. R. Huffman, *Nature* **1990**, *347*, 354.

[3] S. Iijima, *Nature* **1991**, *354*, 56.

[4] P. Ball, *Nature* **2001**, *414*, 142.

[5] M. Monthioux, V. L. Kuznetsov, *Carbon* **2006**, *44*, 1621.

[6] S. Iijima, T. Ichihashi, *Nature* **1993**, *363*, 603.

[7] D. S. Bethune, C. H. Klang, M. S. de Vries, G. Gorman, R. Savoy, J. Vazquez, R. Beyers, *Nature* **1993**, *363*, 605.

[8] P. Avouris, J. Appenzeller, R. Martel, S. J. Wind, *Proc. IEEE* **2003**, *9*, 1772.

[9] Q.-H. Yang, S. Bai, J.-L. Sauvajol, J.-B. Bai, *Adv. Mater.* **2003**, *15*, 792.

[10] X. Wang, Q. Li, J. Xie, Z. Jin, J. Wang, Y. Li, K. Jiang, S. Fan, *Nano Lett.* **2009**, *9*, 3137.

[11] R. Zhang, Y. Zhang, Q. Zhang, H. Xie, W. Qian, F. Wei, *ACS Nano* **2013**, *7*, 6156.

[12] R. Saito, G. Dresselhaus, M. S. Dresselhaus, *Physical Properties of Carbon Nanotubes*, Imperial College Press, **1998**.

[13] S. Reich, C. Thomsen, J. Maultzsch, *Carbon Nanotubes: Basic Concepts and Physical Properties*, John Wiley & Sons, **2004**.

[14] H. B. Ribeiro, K. Sato, G. S. N. Eliel, E. A. T. de Souza, C.-C. Lu, P.-W. Chiu, R. Saito, M. A. Pimenta, *Carbon* **2015**, *90*, 138.

[15] A. Javey, J. Kong, *Carbon Nanotube Electronics*, Springer Science & Business Media, **2009**.

[16] T. Enoki, T. Ando, *Physics and Chemistry of Graphene: Graphene to Nanographene*, CRC Press, **2013**.

[17] J. W. Wilder, L. C. Venema, A. G. Rinzler, R. E. Smalley, C. Dekker, *Nature* **1998**, *391*, 59.

[18] W. Gomulya, Selecting Semiconducting Single-Walled Carbon Nanotubes by Polymer Wrapping: Mechanism and Performances, University of Groningen, **2015**.

[19] R. Saito, M. Fujita, G. Dresselhaus, M. S. Dresselhaus, *Phys. Rev. B* **1992**, *46*, 1804.

[20] N. Hamada, S. Sawada, A. Oshiyama, *Phys. Rev. Lett.* **1992**, *68*, 1579.

[21] V. Derenskyi, Polymer-Wrapped Carbon Nanotubes for High Performance Field Effect Transistors, University of Groningen, **2017**.

[22] J. Prasek, J. Drbohlavova, J. Chomoucka, J. Hubalek, O. Jasek, V. Adam, R. Kizek, *J. Mater. Chem.* **2011**, *21*, 15872.

[23] C. Journet, W. K. Maser, P. Bernier, A. Loiseau, M. L. de la Chapelle, S. Lefrant, P. Deniard, R. Lee, J. E. Fischer, *Nature* **1997**, *388*, 756.

[24] M. Takizawa, S. Bandow, M. Yudasaka, Y. Ando, H. Shimoyama, S. Iijima, *Chem. Phys. Lett.* **2000**, *326*, 351.

[25] M. José-Yacamán, M. Miki-Yoshida, L. Rendón, J. G. Santiesteban, *Appl. Phys. Lett.* **1993**, *62*, 657.
[26] A. Chortos, I. Pochorovski, P. Lin, G. Pitner, X. Yan, T. Z. Gao, J. W. F. To, T. Lei, J. W. Will, H.-S. P. Wong, Z. Bao, *ACS Nano* **2017**, DOI 10.1021/acsnano.7b01076.
[27] L. Wei, B. Liu, X. Wang, H. Gui, Y. Yuan, S. Zhai, A. K. Ng, C. Zhou, Y. Chen, *Adv. Electron. Mater.* **2015**, *1*.
[28] L. C. Qin, *J. Mater. Sci. Lett.* **1997**, *16*, 457.
[29] A. M. Cassell, J. A. Raymakers, J. Kong, H. Dai, *J. Phys. Chem. B* **1999**, *103*, 6484.
[30] H. Dai, *Acc. Chem. Res.* **2002**, *35*, 1035.
[31] K. S. Kim, M. Imris, A. Shahverdi, Y. Alinejad, G. Soucy, *J. Phys. Chem. C* **2009**, *113*, 4340.
[32] O. Smiljanic, B. L. Stansfield, J.-P. Dodelet, A. Serventi, S. Désilets, *Chem. Phys. Lett.* **2002**, *356*, 189.
[33] J. Hahn, J. H. Han, J.-E. Yoo, H. Y. Jung, J. S. Suh, *Carbon* **2004**, *42*, 877.
[34] A. V. Krestinin, N. N. Dremova, E. I. Knerel'man, L. N. Blinova, V. G. Zhigalina, N. A. Kiselev, *Nanotechnologies Russ.* **2015**, *10*, 537.
[35] L. Ding, A. Tselev, J. Wang, D. Yuan, H. Chu, T. P. McNicholas, Y. Li, J. Liu, *Nano Lett.* **2009**, *9*, 800.
[36] J. Li, K. Liu, S. Liang, W. Zhou, M. Pierce, F. Wang, L. Peng, J. Liu, *ACS Nano* **2014**, *8*, 554.
[37] Y. Che, C. Wang, J. Liu, B. Liu, X. Lin, J. Parker, C. Beasley, H.-S. P. Wong, C. Zhou, *ACS Nano* **2012**, *6*, 7454.
[38] J. Zaumseil, *Semicond. Sci. Technol.* **2015**, *30*, 074001.
[39] J. Lefebvre, J. Ding, Z. Li, P. Finnie, G. Lopinski, P. R. L. Malenfant, *Acc. Chem. Res.* **2017**, *50*, 2479.
[40] M. C. Hersam, *Nat. Nanotechnol.* **2008**, *3*, 387.
[41] J. Chen, M. A. Hamon, H. Hu, Y. Chen, A. M. Rao, P. C. Eklund, R. C. Haddon, *Science* **1998**, *282*, 95.
[42] H. Hu, B. Zhao, M. A. Hamon, K. Kamaras, M. E. Itkis, R. C. Haddon, *J. Am. Chem. Soc.* **2003**, *125*, 14893.
[43] M. S. Strano, C. A. Dyke, M. L. Usrey, P. W. Barone, M. J. Allen, H. Shan, C. Kittrell, R. H. Hauge, J. M. Tour, R. E. Smalley, *Science* **2003**, *301*, 1519.
[44] A. Hirsch, *Angew. Chem. Int. Ed.* **2002**, *41*, 1853.
[45] R. Martel, *ACS Nano* **2008**, *2*, 2195.
[46] M. J. O'Connell, S. M. Bachilo, C. B. Huffman, V. C. Moore, M. S. Strano, E. H. Haroz, K. L. Rialon, P. J. Boul, W. H. Noon, C. Kittrell, J. Ma, R. H. Hauge, R. B. Weisman, R. E. Smalley, *Science* **2002**, *297*, 593.
[47] D. A. Tsyboulski, J.-D. R. Rocha, S. M. Bachilo, L. Cognet, R. B. Weisman, *Nano Lett.* **2007**, *7*, 3080.
[48] M. S. Arnold, A. A. Green, J. F. Hulvat, S. I. Stupp, M. C. Hersam, *Nat. Nanotechnol.* **2006**, *1*, 60.
[49] F. Wang, G. Dukovic, L. E. Brus, T. F. Heinz, *Science* **2005**, *308*, 838.

[50] L. Huang, H. Zhang, B. Wu, Y. Liu, D. Wei, J. Chen, Y. Xue, G. Yu, H. Kajiura, Y. Li, *J. Phys. Chem. C* **2010**, *114*, 12095.
[51] S. Ghosh, S. M. Bachilo, R. B. Weisman, *Nat. Nanotechnol.* **2010**, *5*, 443.
[52] H. Liu, D. Nishide, T. Tanaka, H. Kataura, *Nat. Commun.* **2011**, *2*, 309.
[53] T. Tanaka, H. Jin, Y. Miyata, S. Fujii, H. Suga, Y. Naitoh, T. Minari, T. Miyadera, K. Tsukagoshi, H. Kataura, *Nano Lett.* **2009**, *9*, 1497.
[54] R. Krupke, F. Hennrich, H. v Löhneysen, M. M. Kappes, *Science* **2003**, *301*, 344.
[55] S. A. Curran, P. M. Ajayan, W. J. Blau, D. L. Carroll, J. N. Coleman, A. B. Dalton, A. P. Davey, A. Drury, B. McCarthy, S. Maier, A. Strevens, *Adv. Mater.* **1998**, *10*, 1091.
[56] A. Nish, J.-Y. Hwang, J. Doig, R. J. Nicholas, *Nat. Nanotechnol.* **2007**, *2*, 640.
[57] J. Gao, M. A. Loi, E. J. F. de Carvalho, M. C. dos Santos, *ACS Nano* **2011**, *5*, 3993.
[58] W. Gomulya, G. D. Costanzo, E. J. F. de Carvalho, S. Z. Bisri, V. Derenskyi, M. Fritsch, N. Fröhlich, S. Allard, P. Gordiichuk, A. Herrmann, S. J. Marrink, M. C. dos Santos, U. Scherf, M. A. Loi, *Adv. Mater.* **2013**, *25*, 2948.
[59] M. J. Shea, R. D. Mehlenbacher, M. T. Zanni, M. S. Arnold, *J. Phys. Chem. Lett.* **2014**, *5*, 3742.
[60] H. Wang, B. Hsieh, G. Jiménez-Osés, P. Liu, C. J. Tassone, Y. Diao, T. Lei, K. N. Houk, Z. Bao, *Small* **2015**, *11*, 126.
[61] E. Joselevich, C. M. Lieber, *Nano Lett.* **2002**, *2*, 1137.
[62] H. W. Lee, Y. Yoon, S. Park, J. H. Oh, S. Hong, L. S. Liyanage, H. Wang, S. Morishita, N. Patil, Y. J. Park, J. J. Park, A. Spakowitz, G. Galli, F. Gygi, P. H.-S. Wong, J. B.-H. Tok, J. M. Kim, Z. Bao, *Nat Commun* **2011**, *2*, 541.
[63] W. Gomulya, V. Derenskyi, E. Kozma, M. Pasini, M. A. Loi, *Adv. Funct. Mater.* **2015**, *25*, 5858.
[64] V. Derenskyi, W. Gomulya, W. Talsma, J. M. Salazar-Rios, M. Fritsch, P. Nirmalraj, H. Riel, S. Allard, U. Scherf, M. A. Loi, *Adv. Mater.* **2017**.
[65] T. Lei, Y.-C. Lai, G. Hong, H. Wang, P. Hayoz, R. T. Weitz, C. Chen, H. Dai, Z. Bao, *Small* **2015**, *11*, 2946.
[66] I. Pochorovski, H. Wang, J. I. Feldblyum, X. Zhang, A. L. Antaris, Z. Bao, *J. Am. Chem. Soc.* **2015**, *137*, 4328.
[67] F. A. Lemasson, T. Strunk, P. Gerstel, F. Hennrich, S. Lebedkin, C. Barner-Kowollik, W. Wenzel, M. M. Kappes, M. Mayor, *J. Am. Chem. Soc.* **2011**, *133*, 652.
[68] H. W. Lee, Y. Yoon, S. Park, J. H. Oh, S. Hong, L. S. Liyanage, H. Wang, S. Morishita, N. Patil, Y. J. Park, J. J. Park, A. Spakowitz, G. Galli, F. Gygi, P. H.-S. Wong, J. B.-H. Tok, J. M. Kim, Z. Bao, *Nat. Commun.* **2011**, *2*, 541.
[69] S. Z. Bisri, J. Gao, V. Derenskyi, W. Gomulya, I. Iezhokin, P. Gordiichuk, A. Herrmann, M. A. Loi, *Adv. Mater.* **2012**, *24*, 6147.
[70] J. Gao, W. Gomulya, M. A. Loi, *Chem. Phys.* **2013**, *413*, 35.
[71] S. Kahmann, J. M. Salazar Rios, M. Zink, S. Allard, U. Scherf, M. C. dos Santos, C. J. Brabec, M. A. Loi, *J. Phys. Chem. Lett.* **2017**, *8*, 5666.

[72] W. Gomulya, J. M. Salazar Rios, V. Derenskyi, S. Z. Bisri, S. Jung, M. Fritsch, S. Allard, U. Scherf, M. C. dos Santos, M. A. Loi, *Carbon* **2015**, *84*, 66.
[73] R. H. Baughman, A. A. Zakhidov, W. A. de Heer, *Science* **2002**, *297*, 787.
[74] C. Toumey, nnano.2015.318, **2016**.
[75] Q. Cao, J. Tersoff, D. B. Farmer, Y. Zhu, S.-J. Han, *Science* **2017**, *356*, 1369.
[76] S. J. Tans, A. R. M. Verschueren, C. Dekker, *Nature* **1998**, *393*, 49.
[77] M. Kwak, J. Gao, D. K. Prusty, A. J. Musser, V. A. Markov, N. Tombros, M. C. A. Stuart, W. R. Browne, E. J. Boekema, G. ten Brinke, H. T. Jonkman, B. J. van Wees, M. A. Loi, A. Herrmann, *Angew. Chem. Int. Ed.* **2011**, *50*, 3206.
[78] S. Park, M. Vosguerichian, Z. Bao, *Nanoscale* **2013**, *5*, 1727.
[79] V. Derenskyi, W. Gomulya, J. M. S. Rios, M. Fritsch, N. Fröhlich, S. Jung, S. Allard, S. Z. Bisri, P. Gordiichuk, A. Herrmann, U. Scherf, M. A. Loi, *Adv. Mater.* **2014**, *26*, 5969.
[80] P. H. Lau, K. Takei, C. Wang, Y. Ju, J. Kim, Z. Yu, T. Takahashi, G. Cho, A. Javey, *Nano Lett.* **2013**, *13*, 3864.
[81] C. Cao, J. B. Andrews, A. Kumar, A. D. Franklin, *ACS Nano* **2016**, 877.
[82] E. S. Snow, J. P. Novak, P. M. Campbell, D. Park, *Appl. Phys. Lett.* **2003**, *82*, 2145.
[83] S. M. Sze, K. K. Ng, *Physics of Semiconductor Devices*, John Wiley & Sons, **2006**.
[84] F. Jakubka, S. P. Schießl, S. Martin, J. M. Englert, F. Hauke, A. Hirsch, J. Zaumseil, *ACS Macro Lett.* **2012**, *1*, 815.
[85] S. K. Samanta, M. Fritsch, U. Scherf, W. Gomulya, S. Z. Bisri, M. A. Loi, *Acc. Chem. Res.* **2014**, *47*, 2446.
[86] P. G. Collins, K. Bradley, M. Ishigami, A. Zettl, *Science* **2000**, *287*, 1801.
[87] Z. Chen, J. Appenzeller, J. Knoch, Y. Lin, P. Avouris, *Nano Lett.* **2005**, *5*, 1497.
[88] Z. Bao, J. Locklin, G. Horowitz, *CRC Press* **2007**, *10*, 365.
[89] D. Cahen, A. Kahn, E. Umbach, *Mater. Today* **2005**, *8*, 32.
[90] D. Natali, M. Caironi, *Adv. Mater.* **2012**, *24*, 1357.
[91] G. Horowitz, R. Hajlaoui, H. Bouchriha, R. Bourguiga, M. Hajlaoui, *Adv. Mater.* **1998**, *10*, 923.
[92] A. Ortiz-Conde, F. J. García Sánchez, J. J. Liou, A. Cerdeira, M. Estrada, Y. Yue, *Microelectron. Reliab.* **2002**, *42*, 583.
[93] B. Blülle, R. Häusermann, B. Batlogg, *Phys. Rev. Appl.* **2014**, *1*, 1.
[94] D. Braga, G. Horowitz, *Adv. Mater.* **2009**, *21*, 1473.
[95] Q. Cao, M. Xia, C. Kocabas, M. Shim, J. A. Rogers, S. V. Rotkin, *Appl. Phys. Lett.* **2007**, *90*, 2005.
[96] Y. Asada, Y. Miyata, K. Shiozawa, Y. Ohno, R. Kitaura, T. Mizutani, H. Shinohara, *J. Phys. Chem. C* **2011**, *115*, 270.
[97] N. Izard, S. Kazaoui, K. Hata, T. Okazaki, T. Saito, S. Iijima, N. Minami, *Appl. Phys. Lett.* **2008**, *92*, 243112.
[98] J. M. Luther, M. Law, M. C. Beard, Q. Song, M. O. Reese, R. J. Ellingson, A. J. Nozik, *Nano Lett.* **2008**, *8*, 3488.

[99] M. P. Ramuz, M. Vosgueritchian, P. Wei, C. Wang, Y. Gao, Y. Wu, Y. Chen, Z. Bao, *ACS Nano* **2012**, *6*, 10384.
[100] M. J. Shea, M. S. Arnold, *Appl. Phys. Lett.* **2013**, *102*, 243101.
[101] Y. Ye, D. J. Bindl, R. M. Jacobberger, M.-Y. Wu, S. S. Roy, M. S. Arnold, *Small* **2014**.
[102] H. Wang, G. I. Koleilat, P. Liu, G. Jiménez-Osés, Y.-C. Lai, M. Vosgueritchian, Y. Fang, S. Park, K. N. Houk, Z. Bao, *ACS Nano* **2014**, DOI 10.1021/nn406256y.
[103] S. N. Habisreutinger, T. Leijtens, G. E. Eperon, S. D. Stranks, R. J. Nicholas, H. J. Snaith, *Nano Lett.* **2014**.
[104] S. N. Habisreutinger, T. Leijtens, G. E. Eperon, S. D. Stranks, R. J. Nicholas, H. J. Snaith, *J. Phys. Chem. Lett.* **2014**, *5*, 4207.
[105] K. Aitola, K. Domanski, J.-P. Correa-Baena, K. Sveinbjörnsson, M. Saliba, A. Abate, M. Grätzel, E. Kauppinen, E. M. J. Johansson, W. Tress, A. Hagfeldt, G. Boschloo, *Adv. Mater.* **2017**, *29*.
[106] S. N. Habisreutinger, R. J. Nicholas, H. J. Snaith, *Adv. Energy Mater.* **2017**, *7*.